

A single myosin head moves along an actin filament with regular steps of 5.3 nanometres

Kazuo Kitamura*†‡, Makio Tokunaga*§, Atsuko Hikikoshi Iwane†‡ & Toshio Yanagida*†‡||

* Yanagida BioMotron Project, ERATO, JST, 2-4-14 Senba-Higashi, Mino, Osaka 562-0035, Japan

† Department of Biophysical Engineering, Osaka University, 1-3 Machikaneyama, Toyonaka, Osaka 560-8531, Japan

‡ Department of Physiology I, Osaka University Medical School, 2-2 Yamadaoka, Suita, Osaka 565-0871, Japan

§ Structural Biology Center, National Institute of Genetics, Mishima, Shizuoka 411-8540, Japan

|| Single Molecule Processes Project, ICORP, JST, 2-4-14 Senba-Higashi, Mino, Osaka 562-0035, Japan

Actomyosin, a complex of actin filaments and myosin motor proteins, is responsible for force generation during muscle contraction. To resolve the individual mechanical events of force generation by actomyosin, we have developed a new instrument with which we can capture and directly manipulate individual myosin subfragment-1 molecules using a scanning probe. Single subfragment-1 molecules can be visualized by using a fluorescent label. The data that we obtain using this technique are consistent with myosin moving along an actin filament with single mechanical steps of approximately 5.3 nanometres; groups of two to five rapid steps in succession often produce displacements of 11 to 30 nanometres. This multiple stepping is produced by a single myosin head during just one biochemical cycle of ATP hydrolysis.

Studies of the actomyosin motor have entered a new phase in the past few years. Structures of the actin monomer¹ and the myosin head², determined by X-ray crystallography, have provided a framework for understanding the interaction between the myosin head and the actin filament. The ‘tilting crossbridge’ model of force generation^{3,4} has been refined, on the basis of the myosin crystal structure, into the ‘lever-arm’ hypothesis⁵. In this model, small structural changes that are coupled to ATP hydrolysis in the catalytic domain of the myosin head are magnified by pivoting of the ~10-nm-long myosin light-chain domain, which acts as a lever arm^{5–7}. The translation caused by this pivoting of the lever arm would be ~6 nm (refs 8, 9).

New techniques for manipulating single actin filaments using microneedles¹⁰ or optical traps¹¹ and optical sensors that can resolve objects at nanometre scales^{11,12} have allowed the displacement of single molecules of myosin or its subfragments to be measured directly *in vitro*^{11–18}. The size of displacements reported, however, has varied considerably. Some investigators have found myosin displacements of 4–10 nm (refs 11, 14–17), which are consistent with the lever-arm model. On the other hand, we have reported values of 10–25 nm (refs 18–20), which is significantly larger than the values expected from the lever-arm model. Large displacement values indicate that myosin heads may interact several times with an actin filament for each ATP used^{12,21–24}. It is essential to measure the displacement unambiguously to determine how conformational changes in the myosin head lead to force generation, and how mechanical cycles are coupled to ATP hydrolysis.

We have developed a new method for directly manipulating single myosin subfragment-1 (S1) molecules. S1 is the head region of myosin and contains the ATP- and actin-binding sites. The technique uses a scanning probe to measure the mechanical events that occur during generation of actomyosin displacements at high temporal and spatial resolution.

Nano-manipulation of single S1 molecules

The experimental arrangement is shown in Fig. 1a. S1 was biotinylated and fluorescently labelled on the regulatory light chain (RLC) at a molar ratio of >0.95:1 (fluorescent label:RLC). The RLC is a subunit of relative molecular mass 20,000 (20K) that is located near

the carboxy terminus of S1, away from the ATP- and actin-binding sites which are located on the S1 heavy chain. The scanning probe, a 5–7- μm long ZnO crystal whisker^{25,26}, with a very sharp tip (~15 nm radius of curvature), was attached to a fine glass needle mounted on a three-dimensional piezoelectric scanner. The probe was coated with streptavidin so that single myosin heads could be captured specifically at the biotinylation site on the RLC (see Methods). The stiffness of the needles was low (0.01–0.03 pN nm⁻¹), and thus the mechanical load exerted on an S1 molecule was small (<1 pN).

Single S1 molecules captured on the tip of the scanning probe were visualized by objective-type total internal reflection fluorescence microscopy (TIRFM)²⁷, which produced clear images of single fluorophores at a high fluorescence-to-background ratio (Fig. 1b; an individual S1 molecule captured by the probe is identified by an arrowhead). The fluorescence was characterized by a single, approximately gaussian, intensity distribution and single-step photobleaching^{27,28} (data not shown), strongly indicating that the fluorescent spots were indeed due to single fluorophores. The S1 molecule was brought into contact with an actin bundle in the presence of ATP by manipulating the probe (Fig. 1a, right). We detected the displacements resulting from S1–actin interactions by measuring deflections of the needle, with subnanometre accuracy, using a differential pair of photodiodes^{12,18}.

Individual mechanical events

When S1 was not associated with an actin filament, large thermal fluctuations of the probe with an r.m.s. amplitude of ~13 nm were apparent. Upon binding of S1 to actin, the fluctuations decreased suddenly to an r.m.s. amplitude of <4.5 nm (Fig. 2a, upper trace). Motions of the probe caused by S1–actin interactions could be clearly distinguished from thermal noise by monitoring the increase in stiffness¹⁵, calculated as the reciprocal of the variance of the fluctuating probe position (Fig. 2a, lower trace). The concentration of ATP was low (0.1 or 1 μM), leading to prolonged interactions between actin and myosin and thus enabling us to identify individual mechanical events. During S1–actin attachments, the stiffness of the probe–S1–actin linkage increased by more than tenfold to 0.2–1.5 pN nm⁻¹ at 20 °C, and by more than fivefold to

0.1–0.7 pN nm⁻¹ at 27°C. The stiffness at 20°C is similar to estimates of actomyosin crossbridge stiffness (0.5–2 pN nm⁻¹) in intact muscle²⁹. The high stiffness during active generation of displacements greatly improved the instrumental time resolution and signal-to-noise ratio, and allowed us to resolve elementary processes during generation of displacements (see Methods).

Displacements caused by single S1 molecules spread over a wide range of positive and negative values. The large width of this distribution is probably caused by the probe's thermal fluctuations¹⁵; if the S1 molecule attaches to an actin filament when the probe has diffused away from its equilibrium (zero) position, the start position will be displaced. The stiffness started to increase when the needle was displaced to both positive and negative positions, as shown in Fig. 2b, c, respectively. As the start positions are expected to distribute randomly around the zero position, the mean displacement over many events gives the net displacement caused by an S1 molecule¹⁵ (Fig. 2d). The mean displacements, averaged over all of the observed events, were ~13 nm with 0.1 μM ATP (*n* = 55) and ~14 nm with 1 μM ATP (*n* = 135) at 20°C, and ~12 nm (*n* = 235) with 1 μM ATP at 27°C. In some cases (~20%), the direction of the displacement was reversed, probably because the S1 interacted with an actin filament with the opposite orientation in the actin bundle. Therefore, the mean displacements obtained in this way should underestimate the true mean by ~20%. The durations of displacements at 0.1 and 1 μM ATP were distributed exponentially, with means of 2,400 ms (*n* = 55) and 220 ms (*n* = 135), respectively, at 20°C. The second-order rate constant for dissociation of S1–actin by ATP, based on these mean durations, was 4–5 × 10⁶ M⁻¹ s⁻¹, which is consistent with values obtained for an actin–myosin-head complex in solution³⁰ and by optical trapping nanometry^{11,15–20}.

Stepping motion

We scrutinized the rising phase of the displacements to determine the detailed mechanism of sliding. Figure 3 shows the time course of the rising phases on an expanded timescale, in the presence of 1 μM ATP (Fig. 3a) and 0.1 μM ATP (Fig. 3b) at 20°C, and in the presence of 1 μM ATP at 27°C (Fig. 3c). The displacements did not take place abruptly but instead developed in a stepwise fashion. The steps at 20°C were clearer than those at 27°C, because the dwell time between steps was longer.

To analyse the step size for unitary and multiple displacements, we used a statistical method similar to that previously applied for the microtubule-bound molecular motor kinesin³¹ (see Methods). The start point for a step had to have a dwell time of >4 ms, and the variance of the starting position had to be no greater than double that at the final plateau position (Fig. 2b, c). This method excludes steps that have pre-attachment dwell times of <4 ms.

A histogram of pairwise distances during the rising phase of displacements was produced for each record. The data from 66 events obtained in 8 different experiments (50 events from 6 S1 molecules at 1 μM ATP and 16 events from 2 S1 molecules at 0.1 μM ATP) at 20°C were pooled together (Fig. 4a). A new probe was used for each experiment. About 20 events were observed in each experiment. Of the 190 events, 35% (66 events) had a stiffness upon binding of >0.5 pN nm⁻¹; 65% of the events had too small a stiffness to allow us to determine the probe position reliably, and were thus not analysed—when the stiffness upon binding was small, the start positions could not be determined as reliably because of large fluctuations of the probe position. Low stiffness may have occurred when the actin bundle was not rigidly attached to the glass surface or when some actin filaments were not rigidly incorporated into the actin bundle. Data at 27°C were also excluded because the dwell time was short and therefore the start positions could not be reliably determined. The histogram shows a peak spacing at 5.3 ± 0.2 nm (mean ± s.e.m.) and a small shoulder at twice the displacement, ~11 nm. The shoulder is probably caused by the occurrence of two sequential steps within the interval (which was 2 ms) used for calculating the distance histogram (see Methods). A small shoulder was identified near -5 nm. This shoulder may have resulted from backward steps (Fig. 3b). The peak at 5.3 nm in the histogram is statistically significant according to χ² test of goodness of fit and a non-parametric test based on a kernel-type probability density function (see Methods).

Figure 4b shows histograms of dwell times between steps. The data are well fitted by single exponentials with time constants of 3.2 and 4.8 ms in the presence of 0.1 and 1 μM ATP, respectively, indicating that the steps may have occurred stochastically. The mean velocities in the rising phase, obtained from step size divided by dwell time, are 1.7 and 1.1 μm s⁻¹ at 0.1 and 1 μM ATP, respectively, at 20°C. These velocities are close to the maximum sliding velocities between actin and myosin at saturating concentra-

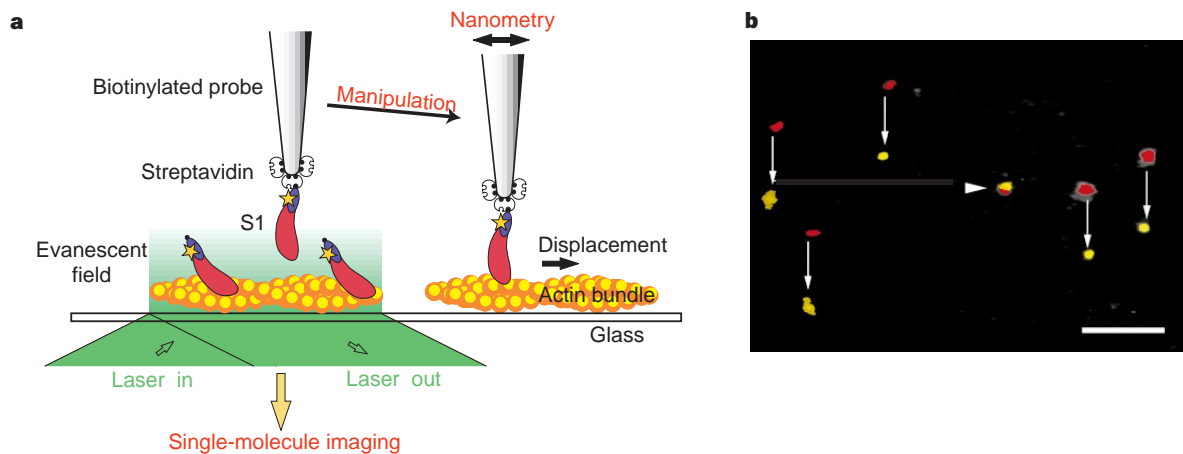


Figure 1 Direct capture and manipulation of a single S1 molecule by a scanning probe. **a**, Schematic drawing of the experiment. Left, a single S1 molecule, which was biotinylated (small black circle) and fluorescently labelled Cy3 (yellow star; molar ratio >0.95:1 Cy3:S1) at its regulatory light chain (blue), was specifically attached at its tail end through the biotin–streptavidin system to a scanning probe (ZnO whisker and glass microneedle) and observed by objective-type TIRFM²⁷. Right, the displacement produced when the S1 molecule was brought into contact with an actin bundle bound to a glass surface was determined by

measuring the position of the needle with nanometre accuracy. See text and Methods for details. **b**, Fluorescence images of single S1 molecules. The micrograph shows superimposed images of single S1 molecules either captured by the probe (arrowheads) or bound to coverslip. The red and yellow spots represent, respectively, images before and after movement of the stage by a piezoelectric actuator. The captured S1 molecule (arrowheads) did not move with the stage, but could be moved independently by piezoelectric scanners holding the needle. Calibration bar, 5 μm.

tions of ATP (>1 mM) and zero load at 20 °C, and are >100-fold larger than the velocities occurring during steady sliding at 0.1 and 1 μM ATP³². The mean velocity (3.1 μm s⁻¹) at 27 °C, obtained from the slope of the rising phase of averaged events (*n* = 35), was roughly twofold larger than that at 20 °C (*Q*₁₀ = 2.7).

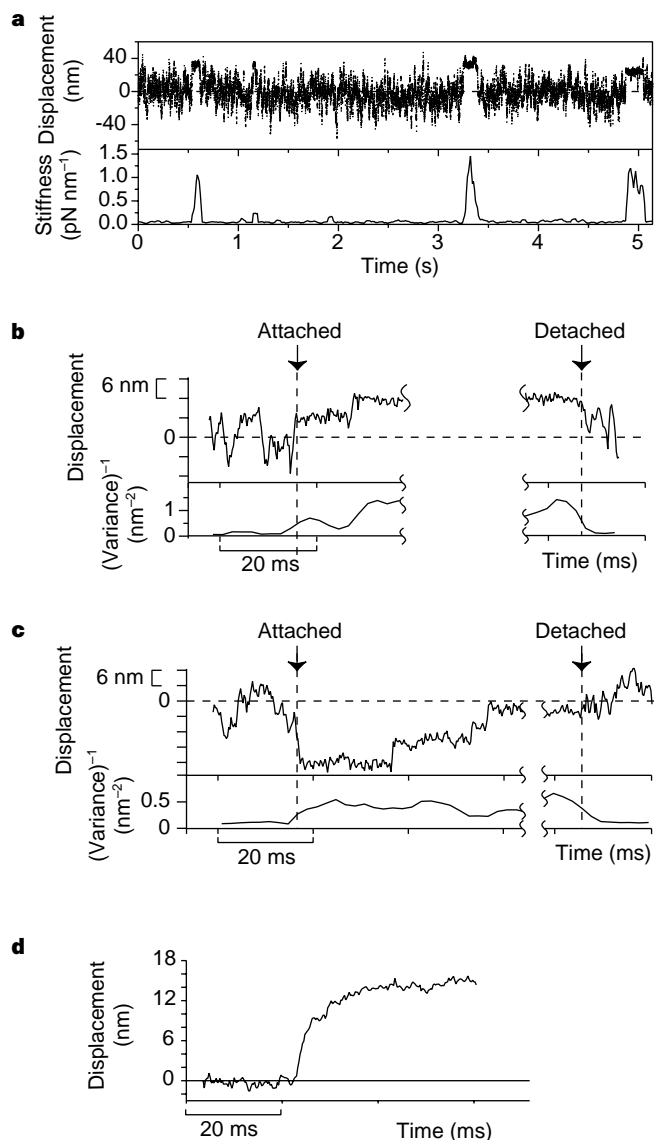


Figure 2 Displacements caused by single S1 molecules captured on the tip of the scanning probe. **a**, Upper trace, typical recordings of the displacements made by an S1 molecule. Bandwidth for recording, 2 kHz. The spring constant of the needle was 0.03 pN nm⁻¹. Lower trace, stiffness calculated at intervals of 20 ms from the variance of the probe position. **b, c**, Displacements due to S1-actin interactions starting at positive (**b**) and negative (**c**) positions. Upper traces, probe-position records plotted on an expanded timescale. Dotted horizontal lines show the equilibrium (zero) position of the probe. Bandwidth, 2 kHz. Lower plots indicate (variance)⁻¹. A 2-ms window was positioned every 1 ms and the variance during the window was calculated from samples at 0.25 ms intervals. In this calculation, the whole range of frequencies of probe fluctuations is not covered because the width of the window (2 ms) was small. 'Attached' and 'detached' indicate attachment and detachment of S1 to actin. **d**, Mean displacement averaged over all observed events (*n* = 135; see text). In averaging the events, we synchronized the start positions of rising phases. As the durations of rising phases varied from event to event, the end positions were not synchronized. Experiments were done in assay buffer containing an oxygen-scavenging system^{10,32} and 1 μM ATP at 20 °C.

The number of steps in each event ranged from one to five, and was 2.5 steps on average (Fig. 4c); that is, the overall displacements ranged from 5.3 to 30 nm and averaged 13 nm. For individual S1 molecules, the distribution of step number ranged from one to three and one to five. The mean displacement (~13 nm) averaged over the events (*n* = 16 + 50, obtained in the presence of 0.1 and 1 μM ATP, respectively) selected for high stiffness at 0.1 and 1 μM ATP at 20 °C was similar to that (~14 nm) averaged over all of the observed events (*n* = 55 + 135). This result indicates that our selection of events for analysis of the steps did not bias the distribution towards large overall displacements.

In the falling phase of the displacements (detachment of the S1 molecule from actin following ATP binding), the probe returned to the zero position with a 1/*e* time of 2–5 ms (Fig. 3a, c, last traces), which was similar to the settling time of the free needle (see Methods). No regular steps were observed either by eye or on a histogram of pairwise distances calculated during the falling phase.

Discussion

In this study, the mean displacement caused by single S1 molecules was 13 nm and displacements of up to 30 nm were observed. These values are greater than those (4–10 nm) reported previously from use of optical trapping nanometry^{11,14–17}. However, in the previous studies, because of the large variance in start positions¹⁵

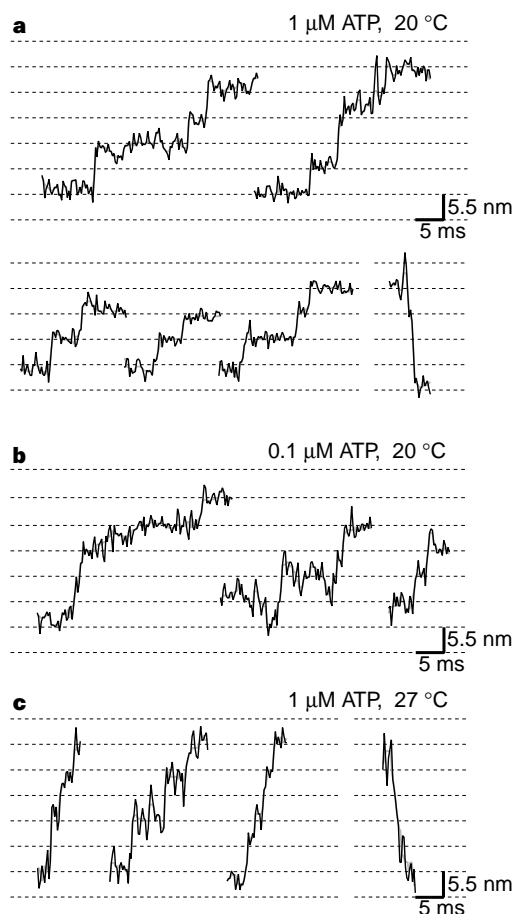


Figure 3 Steps in the rising phase of displacement records on an expanded timescale. Displacements in the presence of **a**, 1 μM ATP, 20 °C; **b**, 0.1 μM ATP, 20 °C; and **c**, 1 μM ATP, 27 °C. Black lines show records passed through a 2-kHz-bandwidth low-pass filter; grey lines show the same records passed through a nonlinear median filter³¹ of rank 2. Dashed horizontal gridlines indicate spacings of 5.5 nm. The start positions of the rising phase of displacements were determined as described in the text. The last traces in **a, c** are records of the falling phase of displacements.

($\pm \sim 30$ nm; r.m.s. ~ 10 nm), only a mean displacement could be determined, rather than the distribution of individual step sizes. Thus, in previous work, some displacements could have been >10 nm. Here we have determined the size of individual displacements directly (Fig. 3). Furthermore, in our study the S1 molecule was brought close to the actin bundle, which was rigidly bound to a glass surface; thus the S1 molecule was more easily able to interact continuously with the actin filaments. In addition, the S1 molecules were specifically attached at their tail ends to the probe by an avidin–biotin system; this avoided damage to the S1 molecules caused by interaction with the probe surface. We have shown previously that the velocity of movement of actin filaments obtained with S1 molecules that are bound to a glass surface through streptavidin–biotinylated BSA, as here, is as fast as the velocity with intact myosin and several fold larger than that obtained when S1 is bound directly to the glass surface³³.

Thermal diffusion of the probe spreads the starting position of displacements, but it cannot account for the number of steps or the large displacements that occur following attachment to actin. In the presence of ADP, the mean displacement was zero and no steps were observed (data not shown). Furthermore, if the displacements resulted from thermal diffusion, the velocity in the rising phase would be proportional to the square root of the absolute temperature. The velocity, however, increased roughly twofold when the temperature was raised from 20 °C to 27 °C (Fig. 3), which is much more than would be expected from thermal diffusion.

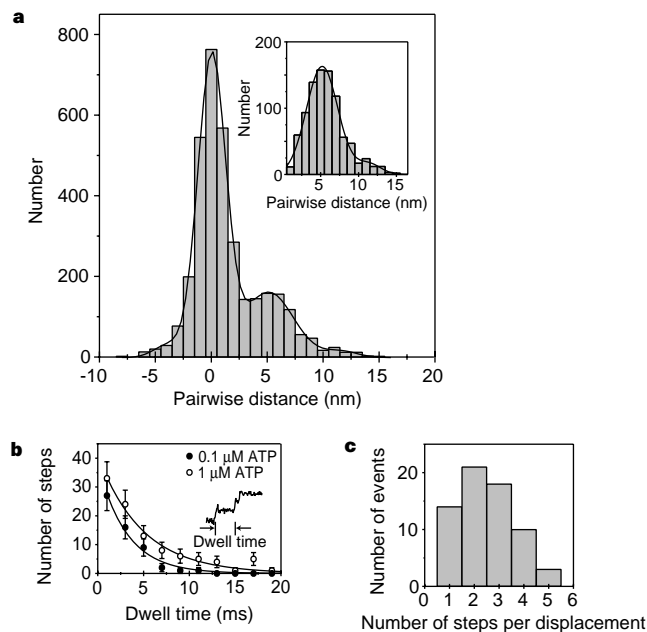


Figure 4 Statistical analysis of stepping motion. **a**, Histogram of pairwise distances in the rising phase of the displacements. The solid line is the sum of four gaussian peaks fitted to the data by least squares⁴⁹. The position and width of each gaussian peak were allowed to vary during the fitting iteration. The fit parameters for positions and widths of four gaussians are -3.8 and 1.3 nm, 0.02 and 1.3 nm, 5.3 and 2.0 nm, 11.3 and 1.6 nm, respectively. Inset, the Gaussian distribution at ~ 0 nm was subtracted from the data and the fitted curve. **b**, Histogram of the dwell times between steps, determined as described²⁵. Values are expressed as $n \pm \sqrt{n}$. Closed and open circles indicate results obtained in the presence of 0.1 and $1 \mu\text{M}$ ATP, respectively. The lines show exponential curves fitted to the data, giving time constants of 3.2 ms and 4.8 ms at 0.1 and $1 \mu\text{M}$ ATP, respectively. **c**, Histogram of the number of steps per displacement. The steps were counted by eye. Steps of $\sim 5.3 \text{ nm} \times N$ were counted as N steps. The histogram shows combined results obtained in the presence of 0.1 or $1 \mu\text{M}$ ATP at 20°C .

We did not observe displacements of more than 30 nm, even though the energy required to produce a 30-nm displacement under the present load ($1/2 \times (30 \text{ nm})^2 \times (0.03 \text{ pN nm}^{-1}) = 14 \text{ pN} \times \text{nm}$) is $<15\%$ of the energy liberated by ATP hydrolysis ($\sim 100 \text{ pN} \times \text{nm}$)³⁴. The displacement may be limited by the helical pitch of actin. If an S1 molecule moves 30 nm along a single strand of an actin filament, the S1 would rotate by $\sim 145^\circ$ around the filament axis. Further rotation may be difficult, because of mechanical constraints at the probe or in the filament bundle.

Could the large displacements composed of successive 5.3-nm steps be produced by multiple S1 molecules? We observed bound fluorophores rather than S1 molecules, so it is possible that the probe may have bound extra, non-fluorescent S1 molecules that were either unlabelled or labelled with photobleached fluorophores. However, this is unlikely, for several reasons. First, S1 molecules, labelled with fluorophores at a molar ratio of $>0.95:1$, were attached to the tip of the probe under safe, red-light illumination (see Methods). Illumination with green laser light was then used to check that single S1 molecules were captured (Fig. 1b). More than 90% of S1 molecules should be fluorescent, at least until this checking procedure is carried out, so most instances of capturing multiple myosins would have been detected by greater fluorescence intensity. Second, the probability of capturing more than one S1 molecule, determined by fluorescence, was $\sim 5\%$ (see Methods) and the fraction of contaminating, non-fluorescent, S1 molecules in the preparation was $<10\%$, so the likelihood that the probe bound one fluorescent S1 molecule and one or more non-fluorescent S1 molecule is $<0.5\%$. Third, if multiple steps are caused by multiple S1 molecules each producing a single step for each ATP used, then the velocity of the rising phase should have been much smaller at $1 \mu\text{M}$ ATP than the actomyosin sliding velocity at a saturating ATP concentration, and should have been lower still in the presence of $0.1 \mu\text{M}$ ATP³². This is because, at low ATP concentrations, the myosin head forms a rigid, long-lived rigor complex with actin that limits the rate of movement.

How are the steps coupled to biochemical cycles of ATP hydrolysis? During the production of one to five steps, to generate displacements of ~ 5 to ~ 30 nm (Fig. 3), the mean dwell times were 3.2 and 4.8 ms in the presence of 0.1 and $1 \mu\text{M}$ ATP, respectively, at 20°C (Fig. 4b). If a single step corresponds to each ATP used, an ATP molecule must bind to the S1 within these dwell times. The likelihood of this is ~ 3.2 ms divided by 2,400 ms and ~ 4.8 ms divided by 220 ms in 0.1 and $1 \mu\text{M}$ ATP, respectively, where 2,400 ms and 220 ms are the average times required for ATP binding, estimated from the plateau durations. If the hydrolysis of a single ATP molecule does correspond to a single step, and if the S1 undergoes more than two steps sequentially, more than two ATP molecules should associate repeatedly with the S1, a much less likely occurrence. The fact that the dwell time did not depend on the ATP concentration indicates that each step did not correlate with the binding of ATP. For kinesin^{35,36} and the F_1 -ATPase³⁷, each translational or rotational step is thought to require hydrolysis of an ATP molecule; for these motor proteins, the dwell times depend strongly on the ATP concentration. Thus, our results indicate that multiple elementary steps may be produced during each biochemical cycle.

The step size coincides approximately with the distance between adjacent actin monomers in one strand of an actin filament (5.5 nm; ref. 38) and myosin heads are known to bind two adjacent actin subunits during rigor⁶. A myosin head may walk along actin by using these two binding sites, without detaching from the filament. Our results do not imply, however, that the myosin head remains continuously attached to actin during movement. The probe and the needle that we used are much larger than S1, and their diffusion rate is slow. If S1 dissociates, it could move or diffuse to the adjacent actin before the probe diffuses away from the actin bundle. Thus, continuous movement along the actin filament or adjacent filaments in the bundle could involve rapid

attachment—(movement)—detachment cycles. Each step may be produced by a conformational change in the myosin head, as suggested by the lever-arm model, or by other mechanisms such as the thermal ratchet (see, for example, ref. 39). It is also possible that conformational changes within the actin filament are important in force generation^{40,41}.

To allow for the production of multiple steps for each molecule of ATP split, chemical energy from ATP hydrolysis might be stored in the myosin head or in the actin filament and released gradually during successive actomyosin interactions. This idea challenges the widely accepted view that force generation is directly coupled to release of bound ligands⁴². We have shown recently that the myosin head can attach to actin and generate force for a considerable time (>100 ms) after the release of bound nucleotide¹⁹. In some other proteins, ligand-induced conformations, termed imprints or protein memory, are retained after removal of the ligand⁴³. Our results indicate that the myosin head may be able to store energy from ATP hydrolysis and later release it productively in several packets of work. □

Methods

Proteins. S1 was obtained by papain digestion of chicken skeletal muscle myosin⁴⁴ and purified by HPLC gel filtration (Superose-6, Pharmacia). Contamination with heavy meromyosin and myosin was below the limit for detection (<0.5%). Biotinylated and fluorescently labelled S1 was obtained by exchanging the RLC for a biotinylated and labelled light chain as described²⁷. A recombinant fusion protein, consisting of biotin-dependent transcarboxylase (BDTC), a peptide biotinylated in *Escherichia coli*, and chicken gizzard myosin RLC, was expressed in *E. coli* strain JM109 and purified³³. The single cysteine residue of RLC was labelled with an orange fluorescing cyanine reagent, Cy3-maleimide, which was prepared by coupling monofunctional Cy3 *N*-hydroxysuccinimide ester (Amersham) with *N*-[2-(1-piperazinyl)ethyl]-maleimide (Dojindo Laboratories, Japan), and Cy3-BDTC-RLC was exchanged for endogenous RLC²⁷. The Cy3:S1 molar ratio was estimated spectrophotometrically from the suspension in solution to be >0.95 using the extinction coefficients $0.83 \text{ (mg/ml)}^{-1} \text{ cm}^{-1}$ at 280 nm for S1 (ref. 44), and $150,000 \text{ M}^{-1} \text{ cm}^{-1}$ at 552 nm for Cy3 (product data sheet). By measuring the absorption of Cy3 in the absence and presence of a twofold molar excess of BDTC-RLC, we found that the extinction coefficient for Cy3 was unchanged (it changed by <2%) upon binding to RLC. The contribution of the absorbance of BDTC to that of S1 was negligible (<1%). To determine whether the suspension was a mixture of S1 molecules that bound none, one and more than one fluorescent Cy3 molecule, we measured the fluorescence intensity and photobleaching of individual S1 molecules bound to a glass surface by TIRFM²⁷. The fluorescence intensity showed a single, approximately gaussian-shaped distribution. 169 out of 179 fluorescent spots, corresponding to S1 molecules, were photobleached in one step, and the other 10 spots were photobleached in two steps. Thus 6% of the S1 molecules apparently bound two dye molecules; this percentage is an upper limit, because two S1 molecules may occasionally have been in close proximity on the coverslip.

Actin⁴⁵ and α -actinin⁴⁶ were obtained from rabbit skeletal muscle and chicken gizzard, respectively. Actin bundles of ~100 nm in width were prepared by dialysis of G-actin and α -actinin in a molar ratio of 10:1 against the assay buffer (25 mM KCl, 5 mM MgCl₂, 20 mM HEPES, pH 7.8), and then fluorescently labelled with BODIPY FL phalloidin (Molecular Probes).

Probe. ZnO whisker crystals (a gift from Central Research Laboratories, Matsushita Electric Industrial Co, Ltd) were amino-silanized as described⁴⁷, biotinylated in *N,N*-dimethylformamide containing 1 mM 5-[5-(*N*-succinimidylloxycarbonyl)pentylamido]hexyl-D-biotinamide (biotin-(AC₅)₂-Osu, Dojindo Laboratories) overnight at room temperature, washed several times with ethanol and stored in ethanol. A biotinylated ZnO whisker was glued with epoxy resin under a binocular microscope to the end of a very fine glass microneedle, ~100 μm long and ~0.3 μm in diameter¹⁸. The bending stiffness (spring constant) of the needles was calibrated by measuring the mean square of their thermal fluctuations using the principle of energy equipartition¹⁸, or by cross-calibration against stiffer calibrated needles¹⁸. The compliance added to the actomyosin-probe-needle system by torsion of the glass needle was

calculated to be 0.5–1 nm pN^{-1} . When the probe was attached directly to a glass surface, fluctuations of the probe were reduced below the detector noise (~0.3 nm r.m.s.), indicating that the ZnO whisker and its epoxy attachment were rigid.

Observation and manipulation of single S1 molecules. Cy3-labelled BDTC-S1 (Cy3-BDTC-S1) was visualized under an improved fluorescence microscope (IMT-2, Olympus) equipped for objective-type TIRFM²⁷ and including a nanometre-piconewton measurement system^{12,18}. Fluorescence intensity and photobleaching were measured under the same conditions as described²⁷. Both the Cy3-labelled S1 and BODIPY-FL-labelled actin bundles were excited by a frequency-doubled Nd:YAG laser ($\lambda = 532 \text{ nm}$)⁴⁸. A solution containing the actin bundles was applied to a glass surface that had been cleaned and then coated with α -actinin (0.1 mg ml^{-1}). Unbound actin bundles were washed out with the assay buffer. $\sim 10^{-16} \text{ mol}$ of Cy3-BDTC-S1 in assay buffer without ATP was then applied to the coverslip. After 1 min of incubation, unbound Cy3-BDTC-S1 was washed out. The surface was then washed with assay buffer containing 0.5% 2-mercaptoethanol and an oxygen-scavenging system^{10,32} to reduce photobleaching. S1 molecules bound to actin bundles fixed on the glass surface were observed briefly (for ~1 s) under 532-nm illumination, a short period compared with the average photobleaching time on actin bundles (~60 s).

The streptavidin-coated probe was then positioned above the surface of a coverslip and scanned over a $1 \mu\text{m} \times 1 \mu\text{m}$ area to capture a single S1 molecule through the streptavidin-biotin bond. Contact of the probe with the surface was monitored by observing thermal fluctuations of the needle, under He-Ne laser ($\lambda = 632.8 \text{ nm}$) illumination. The green laser was turned off during this part of the procedure to suppress photobleaching. Then the fluorescence at the tip of the probe was observed under 532-nm illumination, as described above, to determine, according to the fluorescence intensity and single-step photobleaching²⁷ whether a single S1 molecule had bound. During the time required (~5 min) to complete all experimental manipulations before checking for capture of a single S1, under the red-light and room-lighting conditions used, the number of photobleached Cy3 molecules bound to S1 attached to actin bundles on a glass surface was ~2% (out of 1,000 observed fluorescent spots). If no S1 molecule was captured, the probe was replaced and this procedure was repeated until an S1 molecule was successfully captured. It was rare that more than one S1 molecules was captured, as determined by fluorescence (1 of 20 trials in which S1 molecule(s) were captured). At the S1 concentration, solution and illumination conditions, and duration of the experiments used, we did not observe binding of more than two molecules to the tip of the probe. Damage of an S1 molecule by physical contact with the probe during this process is likely to be small because the needle was very flexible. The stiffness of the needle was >1,000-fold less than that of the cantilevers generally used for scanning probe microscopy (>0.1 nN nm^{-1}). The probe and captured S1 were manipulated in three dimensions, with subnanometre accuracy, by piezoelectric scanners.

Displacement measurements. After the S1 molecule was captured on the probe tip, ATP was added to the medium. The S1 was then brought into contact with a fresh actin bundle bound to a different region of the same coverslip (Fig. 1a). The angle between the needle and the actin bundle was set at ~90°. The interaction between the single S1 molecule and the actin filaments was monitored by measuring deflections of the glass microneedle with subnanometre resolution using a split-photodiode and the 532-nm laser¹⁸. The response time (rise time from 0 to 63% of a free needle was 2–5 ms, as determined from the corner frequency ($f_c = 30\text{--}60 \text{ Hz}$) of the power spectrum of the needle's thermal fluctuations: the response time ($\tau = 1/(2\pi f_c)$). During generation of displacements, however, the stiffness of the probe-S1-actin linkage (k_{s1}) increased, so that τ should be greatly improved according to the equation $\tau = \zeta/(k_{s1} + k_{\text{needle}})$, where ζ is the friction coefficient. τ is calculated to be < 0.4 ms at $k_{s1} > 0.5 \text{ pN nm}^{-1}$. This response time was sufficient to observe steps occurring on a millisecond timescale. Thermal fluctuations of a free needle were large (r.m.s. amplitude ~13 nm), but they decreased during generation of displacements because of the increased stiffness (Fig. 2). This effect can be quantified using the principle of energy equipartition, $\langle x^2 \rangle^{1/2} = (k_B T / (k_{s1} + k_{\text{needle}}))^{1/2}$, where k_B is Boltzmann's constant and T is the absolute temperature. When k_{s1} is $> 0.5 \text{ pN nm}^{-1}$, $\langle x^2 \rangle^{1/2}$ is <2.5 nm, which is small enough not to obscure the stepping motions.

Data acquisition and analysis. Probe position data were acquired at 24 kHz by a DAT recorder (RD-125T, TEAC, Japan), and analysed offline by using DADiSP (DSP Development Corp.), LabVIEW (National Instruments) and Origin (Microcal, Inc.) software. The acquired data were passed through a digital recursive Chebyshev type I filter of bandwidth 2 kHz. Pairwise distances were obtained by a method used previously for determining the step size of kinesin³¹, with some modifications. Before the pairwise-distance analysis, the rising phases of the displacements were further filtered by a nonlinear median filter of rank 2 (ref. 31). The traces during the rising phase were shifted by 2 ms and the distances between the original and shifted traces were calculated every 0.25 ms. Reliability of the signal-processing and statistical analysis was checked by the following observations. When a single S1 molecule attached to the probe was bound to an actin bundle on a glass surface in the absence of ATP and the stage was moved smoothly at a velocity similar to that occurring in the rising phase of the displacements, the pairwise-distance histogram showed a single gaussian peak and no auxiliary peaks at a spatial periodicity near 5.3 nm. As the stage could not be moved in 5.3-nm steps rapidly enough to simulate the active steps, simulated data with stochastic 5.3-nm steps and gaussian noise were processed in the same way as experimental data. The distance histogram was indistinguishable from that shown in Fig. 4a.

Statistics. The sum of several gaussian distributions was fitted to the data by the least-squares method using the Levenberg–Marquardt algorithm⁴⁹. The fitted curve was tested by the χ^2 test of goodness of fit (significance level, $\alpha = 0.005$). The data were further tested by a non-parametric test based on the kernel-type probability-density function (PDF).⁵⁰ The estimator of the PDF is defined as:

$$\hat{f}(x : h) = (nh)^{-1} \sum_{i=1}^n K\left(\frac{x - X_i}{h}\right)$$

where n is the number of the data, X_i is the i th datum and h is the bandwidth that satisfies the relationship $h \propto n^{1/5}$. The standard normal distribution function has been used as the kernel $K(\cdot)$. The sign of the differential coefficient of the PDF shows the increase or the decrease of the PDF which indicates the position of the peaks within the PDF.

Received 17 March; accepted 1 December 1998.

1. Kabsch, W., Mannherz, H. G., Suck, D., Pai, E. F. & Holmes, K. C. Atomic structure of the actin: DNase I complex. *Nature* **347**, 37–44 (1990).
2. Rayment, I. et al. Three-dimensional structure of myosin subfragment-1: a molecular motor. *Science* **261**, 50–58 (1993).
3. Huxley, H. E. The mechanism of muscular contraction. *Science* **164**, 1355–1366 (1969).
4. Huxley, A. F. & Simmons, R. M. Proposed mechanism of force generation in striated muscle. *Nature* **233**, 533–538 (1971).
5. Spudich, J. A. How molecular motors work. *Nature* **372**, 515–518 (1994).
6. Rayment, I. et al. Structure of the actin-myosin complex and its implications for muscle contraction. *Science* **261**, 58–65 (1993).
7. Fisher, A. J. et al. X-ray structures of myosin motor domain of *Dictyostelium discoideum* complexed with MgADP·BeF₃ and MgADP·AlF₄. *Biochemistry* **34**, 8960–8972 (1995).
8. Cooke, R. Actomyosin interaction in striated muscle. *Physiol. Rev.* **77**, 671–697 (1997).
9. Howard, J. Molecular motors: structural adaptations to cellular functions. *Nature* **389**, 561–567 (1997).
10. Kishino, A. & Yanagida, T. Force measurements by micromanipulation of a single actin filament by glass needles. *Nature* **334**, 74–76 (1988).
11. Finer, J. T., Simmons, R. M. & Spudich, J. A. Single myosin molecule mechanics: piconewton forces and nanometre steps. *Nature* **368**, 113–119 (1994).
12. Ishijima, A., Doi, T., Sakurada, K. & Yanagida, T. Sub-piconewton force fluctuations of actomyosin *in vitro*. *Nature* **352**, 301–306 (1991).
13. Ishijima, A. et al. Single-molecule analysis of the actomyosin motor using nano-manipulation. *Biochem. Biophys. Res. Commun.* **199**, 1057–1063 (1994).
14. Miyata, H. et al. Stepwise motion of an actin filament over a small number of heavy meromyosin molecules is revealed in an *in vitro* motility assay. *J. Biochem. (Tokyo)* **115**, 644–647 (1994).
15. Molloy, J. E., Burns, J. E., Kendrick-Jones, J., Tregear, R. T. & White, D. C. S. Movement and force produced by a single myosin head. *Nature* **378**, 209–212 (1995).
16. Guilford, W. H. et al. Smooth muscle and skeletal muscle myosins produce similar unitary forces and displacements in the laser trap. *Biophys. J.* **72**, 1006–1021 (1997).

17. Mehta, A. D., Finer, J. T. & Spudich, J. A. Detection of single-molecule interaction using correlated thermal diffusion. *Proc. Natl Acad. Sci. USA* **94**, 7927–7931 (1997).
18. Ishijima, A. et al. Multiple- and single-molecule analysis of the actomyosin motor by nanometer-piconewton manipulation with a microneedle: unitary steps and forces. *Biophys. J.* **70**, 383–400 (1996).
19. Ishijima, A. et al. Simultaneous observation of individual ATPase and mechanical events by a single myosin molecule during interaction with actin. *Cell* **92**, 161–171 (1998).
20. Tanaka, H., Ishijima, A., Honda, M., Saito, K. & Yanagida, T. Orientation dependence of displacements by a single one-headed myosin relative to the actin filament. *Biophys. J.* **75**, 1886–1894 (1998).
21. Yanagida, T., Arata, T. & Oosawa, F. Sliding distance of actin filament induced by a myosin crossbridge during one ATP hydrolysis cycle. *Nature* **316**, 366–369 (1985).
22. Harada, Y., Sakurada, K., Aoki, T., Thomas, D. D. & Yanagida, T. Mechanochemical coupling in actomyosin energy transduction studied by *in vitro* movement assay. *J. Mol. Biol.* **216**, 49–68 (1990).
23. Higuchi, H. & Goldman, Y. E. Sliding distance between actin and myosin filaments per ATP molecule hydrolysed in skinned muscle fibres. *Nature* **352**, 352–354 (1991).
24. Lombardi, V., Piazzesi, G. & Linari, M. Rapid regeneration of the actin-myosin power stroke in contracting muscle. *Nature* **355**, 638–641 (1992).
25. Kitano, M., Hamabe, T., Maeda, S. & Okabe, T. Growth of large tetrapod-like ZnO crystals. *J. Crystal Growth* **102**, 965–973 (1990).
26. Kado, H., Yokoyama, K. & Tohda, T. Atomic force microscopy using ZnO whisker tip. *Rev. Sci. Instrum.* **63**, 3330–3332 (1992).
27. Tokunaga, M., Kitamura, K., Saito, K., Iwane, A. H. & Yanagida, T. Single molecule imaging of fluorophores and enzymatic reactions achieved by objective-type total internal reflection fluorescence microscopy. *Biochem. Biophys. Res. Commun.* **235**, 47–53 (1997).
28. Funatsu, T., Harada, Y., Tokunaga, M., Saito, K. & Yanagida, T. Imaging of single fluorescent molecules and individual ATP turnovers by single myosin molecules in aqueous solution. *Nature* **374**, 555–559 (1995).
29. Huxley, A. F. & Tideswell, S. Filament compliance and tension transients in muscle. *J. Muscle Res. Cell Motil.* **17**, 507–511 (1996).
30. Woledge, R. C., Curtin, N. A. & Homsher, R. *Energetic Aspects of Muscle Contraction* Ch. 3 (Academic, London, 1985).
31. Svoboda, K., Schmidt, C. F., Schnapp, B. J. & Block, S. M. Direct observation of kinesin stepping by optical trapping interferometry. *Nature* **365**, 721–727 (1993).
32. Harada, Y., Noguchi, A., Kishino, A. & Yanagida, T. Sliding movement of single actin filaments on one-headed myosin filaments. *Nature* **326**, 805–808 (1987).
33. Iwane, A. H., Kitamura, K., Yokunaga, M. & Yanagida, T. Myosin subfragment-1 is fully equipped with factors essential for motor function. *Biochem. Biophys. Res. Commun.* **230**, 76–80 (1997).
34. Bagshaw, C. R. *Muscle Contraction* (Chapman & Hall, London, 1993).
35. Kojima, H., Muto, E., Higuchi, H. & Yanagida, T. Mechanics of single kinesin molecules measured by optical trapping nanometry. *Biophys. J.* **73**, 2012–2022 (1997).
36. Schnitzer, M. J. & Block, S. M. Kinesin hydrolyses one ATP per 8-nm step. *Nature* **388**, 386–390 (1997).
37. Yasuda, R., Noji, H., Kinoshita, K. Jr & Yoshida, M. F₁-ATPase is a highly efficient molecular motor that rotates with discrete 120° steps. *Cell* **93**, 1117–1124 (1998).
38. Huxley, H. E. & Brown, W. The low-angle x-ray diagram of vertebrate striated muscle and its behavior during contraction and rigor. *J. Mol. Biol.* **30**, 383–434 (1967).
39. Astumian, R. D. Thermodynamics and kinetics of a brownian motor. *Science* **276**, 917–922 (1997).
40. Egelman, E. H., Francis, N. & DeRosier, D. J. F-actin is a helix with a random variable twist. *Nature* **298**, 131–135 (1982).
41. Yanagida, T., Nakase, M., Nishiyama, K. & Oosawa, F. Direct observation of motion of single F-actin filaments in the presence of myosin. *Nature* **307**, 58–60 (1984).
42. Lynn, R. W. & Taylor, E. W. Mechanism of adenosine triphosphate hydrolysis by actomyosin. *Biochemistry* **10**, 4617–4624 (1971).
43. Klibanov, A. M. Enzyme memory. What is remembered and why? *Nature* **374**, 596 (1995).
44. Margossian, S. S. & Lowey, S. Preparation of myosin and its subfragments from rabbit skeletal muscle. *Methods Enzymol.* **85**, 55–71 (1982).
45. Spudich, J. A. & Watt, S. The regulation of rabbit skeletal muscle contraction. I. Biochemical studies of the interaction of the tropomyosin-troponin complex with actin and the proteolytic fragments of myosin. *J. Biol. Chem.* **246**, 4866–4871 (1971).
46. Craig, S. W., Lancashire, C. L. & Cooper, J. A. Preparation of smooth muscle α -actinin. *Methods Enzymol.* **85**, 316–321 (1982).
47. Tokunaga, M., Aoki, T., Hiroshima, M., Kitamura, K. & Yanagida, T. Subpiconewton intermolecular force microscopy. *Biochem. Biophys. Res. Commun.* **231**, 566–569 (1997).
48. Saito, K., Tokunaga, M., Iwane, A. H. & Yanagida, T. Dual color microscopy of single fluorophores bound to myosin interacting with fluorescently-labelled actin using anti-Stokes fluorescence. *J. Microsc.* **188**, 255–263 (1997).
49. Bevington, P. R. & Robinson, D. K. *Data Reduction and Error Analysis for the Physical Sciences* (McGraw-Hill, New York, 1992).
50. Wand, M. P. & Jones, M. C. *Kernel Smoothing* (Chapman & Hall, London, 1995).

Acknowledgements. We thank T. Funatsu, K. Saito, H. Higuchi, A. Ishijima and H. Kojima for technical suggestions; Y. Ishii and other colleagues of the ERATO project and Osaka University for valuable discussions; A. F. Huxley, Y. E. Goldman, F. Brozovich, C. R. Bagshaw, J. E. Molloy, A. D. Mehta, R. D. Vale and J. West for critically reading the manuscript; S. Kimura for instructions on preparing α -actinin; M. Taniguchi for advice on statistical analysis; and M. Kitano, H. Kado and H. Ogawa for the gift of the ZnO whiskers. This work was partially supported by JSPS Research Fellowships for Young Scientists (K.K.).

Correspondence and requests for materials should be addressed to T.Y. (e-mail: yanagida@phys1.med.osaka-u.ac.jp).